Natural evolution mechanisms of the IDH mutant glioma revealed by multi-omics sequencing of a long-term survivor

Long Wang (wanglong100@aliyun.com)
First Affiliated Hospital of Third Military Medical University: Southwest Hospital https://orcid.org/0000-0002-1395-2444

Feilong Zhao
First Affiliated Hospital of Third Military Medical University: Southwest Hospital

Xuegang Li
First Affiliated Hospital of Third Military Medical University: Southwest Hospital

Tunan Chen
First Affiliated Hospital of Third Military Medical University: Southwest Hospital

Hua Feng
First Affiliated Hospital of Third Military Medical University: Southwest Hospital

Tonghui Ma
First Affiliated Hospital of Third Military Medical University: Southwest Hospital

Fei Li
First Affiliated Hospital of Third Military Medical University: Southwest Hospital

Research Article

Keywords: Tumor evolution, LGG, secondary GBM, IDH, MSP-RON, Immune evasion

Posted Date: March 4th, 2021

DOI: https://doi.org/10.21203/rs.3.rs-281275/v1

Abstract

Purpose Low-grade gliomas(LGG) almost invariably progress into secondary glioblastoma with limited therapeutic options. The currently proposed progression mechanisms were mainly based on treatment intervened patients, seldom is known about the mechanisms under natural evolution.

Methods A high-grade glioblastoma (G4) occurred at the posterior of the primary LGG (G2) of a 67-year-old woman carried the glioma for eight years without any serious treatment. Tumor samples and peripheral blood of the patients were collected and subjected to integrated genomic analyses, including whole-exome sequencing, gene expression and DNA methylation profiling.

Results The center and edge of the tumor were diagnosed as LGG and GBM, respectively. They shared the same trunk mutations including IDH, TP53, and ATRX. They both have mixing cell origins and they have a highly correlated methylation level at the probe level. CIC, BRCA2, and RPA4 mutation which occurred only in G4 with mutant allele frequency(MAF) higher than 15% may contribute to evolution. NAF1 of which the MAF increased by 70% and the mutant RNA reads nearly doubled in G4 may also involve in the evolution. In the pathway level, the MSP-RON pathway was strongly up-regulated in G4. Concomitant with the tumor evolution, we discovered enhanced inflammatory signals represented by the up-regulation of the NF-κB pathway and the recruitment of mast cell, of which the absolute cell proportion increased from 3.9% to 6.9%. Contradictorily, the adaptive immune response was suppressed as we found pathways associated with IL17, dendritic cells, and cytotoxic T cells were down-regulated and the infiltration level of CD4+ and CD8+ T cells were both decreased. As for the TCR profile, only about 2% of blood clonotypes were detected in the tumor microenvironment. Nevertheless, two clonotypes were found significantly expanded. Clone frequencies of them were 38% and 19% in G2, respectively. And these were 24% and 11% in G4, respectively.

Conclusion. Mutation of CIC, BRCA2, RPA4, and NAF1 and activation of the MSP-RON pathway could promote glioma evolution under natural conditions. Increased inflammatory response and decreased adaptive immune response may also contribute to the process. Besides, two highly expanded TCR clonotypes discovered in this case may serve as a potential adoptive cell therapy source in glioma.

Introduction

Gliomas are a heterogeneous group of brain tumors with distinct biological and clinical properties[1,2]. Subtypes and grades of gliomas were defined by histological features traditionally. The 2016 update to the World Health Organization (WHO) classification of tumors integrated molecular and phenotypic features into the classification of glioma. *IDH1/2* mutation, as well as codeletion of 1p/19q, indicates a better prognosis[3,4]. Meanwhile, transcriptome analyses of glioma have classified them into four subtypes denoted proneural, mesenchymal, classical, and neural[5–8], which were correlated with different neural lineages and drug sensitivity. Representative molecular biomarkers of the four subtypes were *EGFR*, *NF1*, *PDGFRA*, and *IDH1*, respectively. However, in some cases boundaries of the four subtypes were blurred in

that a sample might show patterns of more than one subtype[5–9]. Furthermore, several epigenetic markers have also shown prognostic and/or predictive values[10,11]. O6-methylguanine-DNA methyltransferase (*MGMT*) and cytosine-phosphate-guanine (CpG) island methylator phenotype (CIMP) were the two biomarkers that were wildly studied. CIMP was closely correlated with *IDH* for nearly all IDH-mutant gliomas were CIMP[10,12,13]. Recently, two subsets of IDH-mutant/CIMP gliomas were discovered, CIMP-low and CIMP-high. The former presented a relatively low degree of DNA methylation and poorer outcome compared to the latter[10,12–14].

Low-grade gliomas (LGG) almost invariably progress into secondary glioblastoma (sGBM) within 5–10 years after diagnosis[15–17]. sGBM accounts for about 20% of GBM and is generally identified by harboring *IDH* mutation[15,18]. Although the evolutionary landscape[19,20] of GBM has been widely studied, the mechanisms behind remain elusive. Bai and colleagues[21] compared the progressed GBM samples to their lower-grade counterparts in 41 *IDH* mutant glioma patients. They found nonlinear clonal expansion of the original tumors and identified some key oncogenic pathways that drive progression, including activation of the *MYC* and RTK-RAS-PI3K pathways. Besides alterations in oncogenic pathways, local immunosuppression also plays an important role in glioma progression[22–25]. As well-known, glioma presents a more immunosuppressive tumor microenvironment compared with other tumors. Fewer leukocytes infiltration caused by blood-brain-barrier is the main reason. T cell exhaustion and apoptosis via PD-1 ligands (PD-L1/2) expressed by tumor cells also play a role[26]. Effector T cells could be silenced by a combination of soluble factors, such as IL10 and TGFb[22,27,28], and be inhibited by myeloid-derived suppressor cells (MDSCs, $CD33^{+}$ HLA-DR), tumor-associated macrophages, and regulatory T cells (Tregs)[29]. Furthermore, Mohme, et al.[22] identified a distinct exhaustion signature in tumor-infiltrating lymphocytes (TILs) compared to peripheral blood lymphocytes (PBLs) and discovered a contracted repertoire of TCR in recurrent GBM compared to newly diagnosed GBM.

Although a variety of mechanisms have been proposed to clarify glioma progression, all of them are based on the comparison of surgically resected specimens at diagnosis and at relapse, and a majority of them included patients who received chemo/radio therapy, which reflected the artificial selection. How gliomas evolve under natural conditions remains unknown. Here, we try to answer this question by comparing the multi-omics sequencing data of LGG and GMB specimens resected simultaneously from a long-term survivor who carried a tumor for more than eight years without any formal medical interference.

Materials And Methods

Biospecimen acquisition and histological diagnosing

The two adjacent tumors were resected surgically and were applied to histological examination separately. Tumor purity was evaluated histologically. Antibodies used in IHC staining included Anti-ATRX antibody (ID: Sc-55584, Santacruz), Anti-Ki67 antibody (ID: ab15580, Abcam), and Anti-Olig2 antibody (ID: ab109186, Abcam). DNA and RNA of the tumor were extracted using AllPrep DNA/RNA Mini Kit

(ID: 80204, QIAGEN). Peripheral blood of the patient was collected using tubes coated with EDTA before surgery, then DNA was purified from the white blood cells (WBC) centrifuged.

Whole exome sequencing and analyzing

Exonic regions of DNA were captured in a solution using the Agilent SureSelect approach according to the manufacturer's instructions (Agilent, Santa Clara, CA). Paired-end sequencing was performed using the HiSeq X Ten next-generation sequencing instrument (Illumina, San Diego, CA). The average data output was about 200×coverage. Somatic variants were identified using GATK Best Practices Pipeline[30]. Somatic single-nucleotide variants (SNVs) were detected using MuTect[31], while somatic indels were identified using Strelka[32]. Cancer cell fraction was inferred using EXPANDAS[33], clone phylogeny between different samples was estimated by CITUP[34], and was visualized by TimeScape[35].

mRNA sequencing and analyzing.

RNA was isolated and sequenced. The reads were aligned to the Ensembl GRCh37 human genome assembly with default parameters. And were normalized by FPKM. Tumor purity was evaluated by ESTIMATE[36] using FPKM. ssGSEA was performed using the R package GSVA[37]. Transcriptomic profiles of the two tumors were compared using ssGSEA based on three collections of annotated gene sets from the Molecular Signature Database v7.1 (C6 oncogenic genesets, C7 immunologic genesets, and BIOCARTA subset of Canonical pathways of C2) [38]. Cell origins of the two tumors were estimated by ssGSEA using signatures defined by Cahoy et al[39], transcription subtypes of the two samples were inferred using signatures discovered by Verhaak et al[5].

Genome-wide methylation array sequencing and analyzing

Genome-wide DNA methylation measurements were performed on DNA extracted from the two tumors with the Infinium MethylationEPIC BeadChip (Illumina, San Diego, CA, USA). Raw methylation data were preprocessed using the R package minfi[40]. CpG sites with detection p-value >0.01 were regarded as failed and were assigned as missing. Methylation level was reported as beta value and was normalized using BMIQ (Beta MIxture Quantile dilation)[41]. The methylation status of *MGMT* was determined by MGMT-STP27 mode, which calculated the methylation probability using the linear algebra of beta values of two probes cg12434587 and cg12981137[42-44]. CIMP status was evaluated using the signature defined by Noushmehr, et al[14], while CIMP-High status was determined using the signature defined by Ceccarelli, et al[13].

T cell receptor (TCR) sequencing and analyzing

DNA purified from the two tumors and peripheral blood was analyzed by high-throughput sequencing of the full length of TCRβ chain by the ImmuHub™ TCR profiling system (ImmuQuad Biotech, Hangzhou, China). Briefly, sequencing was performed on an Illumina MiSeq® system with PE300 mode (Illumina,

San Diego, California, the USA). MiTCR (milaboratory) algorithm was applied to raw sequencing data for PCR and sequencing error correction and V, D, J, C gene segments mapping with IMGT®. The resulting nucleotide and amino acid sequences of CDR3 of TCRβ chain were determined and those with out-of-frame and stop codon sequences were removed from the identified TCRβ repertoires. The Clonality Index specialized in characterizing the state of clonal proliferation of T cells and the Shannon Index utilized to evaluate clonotype diversity was calculated as previously reported[45].

Data visualization

Figures were visualized using matplotlib 3.2.1 except for the evolutionary tree which was drawn using the R package TimeScape.

Results

Clinical presentation and histopathological considerations

A 67-year-old woman, of whom an intracranial lesion was detected and a closer follow-up observation was prescribed in June 2010. In October 2013, a low-density area with a suborbicular shadow was observed at the right frontal lobe. Attributed to a variety of reasons including no deteriorating symptoms, she didn't receive any formal medical care. In May 2018, she suffered aggravated symptoms, imaging examination showed the tumor at the right frontal lobe increased, while a new enhanced shadow appeared at the posterior of the primary tumor, which indicated the occurrence of a secondary higher-grade glioma there (Fig.1A). The primary and secondary tumors were resected and diagnosed as grade II diffuse astrocytoma (G2 in abbreviation) and grade IV glioblastoma (G4 in abbreviation), respectively. The immunohistochemical result showed that Ki67 expression was higher in G4 than in G2, Olig-2 (oligodendrocyte transcription factor 2) expression was positive in both samples and was higher in G4 (Fig.1B).

The molecular origin of G4

Clinical trajectory suggested that the G4 originated from G2. We explored it at the molecular level. Tumor purity of G2 and G4 were both 100% evaluated histologically, and those were 97% and 96% separately estimated by ESTIMATE(36), which guaranteed the comparability of them. A total of 117 and 96 somatic mutations were detected in G2 and G4, respectively. Among them, 53 mutations were shared between the two samples (Fig.2A). Of note, Minor allele frequencies (MAF) of glioma driver genes *IDH*(p.R132S), *TP53*(p.R234C), and *ATRX*(p.T1582NfsTer19) were approximately equal between the two samples (Fig. 2B). *TERT* promoter mutations, *EGFR* VIII fusion, and 1p/19q co-deletion were detected in neither samples. Therefore, the mutation subtypes of these two specimens were both *IDH* mutant and 1p/19q non-codel, which were consistent with the characteristics of diffuse astrocytoma.

Transcriptionally, *IDH* mutations suggested these two tumors were of proneural subtype. ssGSEA analysis using the signature defined by Verhaak et al.[5] verified the result, proneural got the highest score among

the four transcription subtypes in both samples, which was 32.4% in G2 and 32.8% in G4. However, ssGSEA scores of the rest three transcriptional subtypes were also comparable, which implied the mixing subtypes (Fig.2C). And cell of origin estimated by ssGSEA using signature defined by Cahoy et al.[39] also favored that both samples were of mixing cell origination. Oligodendrocytes accounted for 28.7% and 29.4% in G2 and G4 separately, while astrocytes accounted for 26.6% and 28.3% in G2 and G4 separately (Fig.2C).

At the methylation level, beta values at all CpG loci of G2 and G4 were highly correlated, with R^2 equals 0.991. And only 4,035 out of 761,759 CpGs showed a difference in beta value greater than 0.2 between these two samples (Fig.2D). *MGMG* promoter status of G2, as well as that of G4, was methylated, with the probability of methylated status equals 0.99 estimated by MGMT-STP27 mode for both samples. Epigenetic subtype analysis revealed that both samples were CIMP+ as the probability density of beta-values of probes used to define CIMP+ reached a peak when the beta-value was about 0.76, which was in accordant with that both samples were *IDH* mutant (Fig.2E). Furthermore, both samples were CIMP-high as the majority of beta-values of probes utilized to define CIMP-high distributed around 0.75 (Fig.2F).

Tumor evolution trajectory from G2 to G4

43 mutations were identified only in G4 (private mutations, Fig.3A). Among them, *CIC* mutation (p.Thr761LeufsTer163) had a MAF of 23.3%, and at the transcription level, mutant *CIC* reads accounted for 10% of overall *CIC* reads detected in RNA sequencing. Two genes *RPA4* (p.S2IfsTer50) and *BRCA2* (p.M3217V), which were related to homologous recombinations (HR) pathway, had MAFs of 24% and 15.4%, respectively.

Seven clones were identified (Fig.3B, Table 1). Driver genes with high MAF including *IHD, TP53,* and *NAF1* were all assigned to clone 1, which was the earliest event. Of note, the N219K mutation of *NAF1* has never been reported before. MAF of it increased from 44.4% in G2 to 75.0% in G4, and the proportion of the mutant RNA reads increased from 37.5% to 70.0%, correspondingly. Clone 2, which was also an early event, composed the second-largest cell population in G4. *NOTCH1*(p.A1967V) mutation, of which MAF increased from 20.5% in G2 to 37.5% in G4, was assigned to this clone. Clone 4 was the biggest in G4, and private mutations of G4 including *CIC, BRCA2,* and *MMRN1* were all assigned to this clone, indicating their role in tumor progression. Clone 5 was a new event in G4, MAF of all genes assigned to this clone was less than 10%, except FFAR1 (p.A17V). Contradictorily, clone 6 and clone 7, which occurred in G2, were almost eliminated in G4.

Oncogenic pathways of the two samples were further compared by ssGSEA. Pathways of which the absolute difference of normalized enrichment score (NES) calculated between G4 and G2 was greater than 20% of the NES of G2 were analyzed. (Fig.3C). The highest up-regulated pathway in G4 was the MSP-RON pathway, activation of which can stimulate the Ras-PI3K signaling pathway(46) which was reported to be altered in 68% of recurrent glioma patients(21). The second up-regulated pathway in G4 was the nuclear factor-κB (NF-κB) pathway, activation of which could enhance cancer cell proliferation

and induce immunosuppression. Contrarily, the down-regulated pathways included the dendritic cell pathway, which can stimulate Th1 and Th2 cell differentiation, IL17 pathway, and cytotoxic T cell pathway, indicating the immunosuppression in G4.

Immune microenvironment alteration concomitant with tumor evolution

Immune cell fraction in the two tumors was deconstructed using CIBERSORT(47) (Fig.4A). The infiltration levels of activated mast cells, memory B cell, and follicular helper T cell were higher in G4 (Fig.4A), suggesting their role in defending glioma progression. However, The infiltrations of resting CD4+ memory and CD8+ T cells were decreased in G4 noteworthily, which was consistent with the down-regulation of Th1, Th2, Th17, and cytotoxic T cell pathway aforementioned and implied the evasion of the adaptive immune response in G4.

TCR sequencing of the two tissue samples and peripheral blood was performed to profile epitope recognition patterns during glioma evolution. Of the 1926 clonotypes discovered in peripheral blood, only 42 (2.13%) were detected in G2 or G4 (Fig.4B). Diversity estimated by Shannon-Index was higher in G4 than in G2, correspondingly, clonality was lower in G4 than in G2, which suggested the occurrence of new epitopes during glioma evolution. 15 clonotypes were identified in common between G2 and G4 (Fig.4C), which accounted for 13.2% and 11.4% of all clonotypes of G2 and G4 separately. clone frequencies of all these shared clonotypes were decreased from G2 to G4. Among them, two clonotypes (CASGDRVSWGYTF and CASSLSRGQLNGYTF) had the highest clone frequency in all of G2, G4, and peripheral blood (Fig.4C-D).

Discussion

This case had drawn our attention because a secondary glioblastoma appeared beside the primary LGG without any formal treatment interference in eight years, which enabled us to explore the evolution mechanisms of glioma under natural conditions. Both of the two tumors harbored driver mutations including *IDH*, *TP53*, and *ATRX*, mixing cell origins, and of CIMP-High, which guaranteed that the G4 originated from G2. Two processes were generally considered to contribute to the progression, tumor intrinsic proliferation, and host immune suppression.

Tumor evolution trajectory revealed that clone 4 composed of private mutations in G4 mainly expanded most. Among them, *CIC* mutation indicates the proliferation of oligodendrocytes, *RPA4* and *BRCA2* mutations suggest the inactivation of DNA damage repair pathway. Clone 1, which was the earliest event, included tumor cells harboring *IDH*, *TP53*, and *NAF1* mutations. The p.N219K of *NAF1* has not been recorded in COSMIC and was firstly reported in this case to our knowledge. N219K locates at the Cbf5-binding domain of *NAF1*. The function of this mutation is unknown, however, as MAF of *NAF1* mutation increased nearly 70% and the proportion of mutant RNA reads of *NAF1* increased by about 90%, this mutation probability supplied growth advantage. And overexpression of NAF1 was reported to promote tumorigenesis and progression of glioma through modulating ribosome assembly and protein

synthesis[48]. At the pathway level, we found the activation of the MSP pathway played an important role in the natural progression of glioma. MSP is the ligand for the receptor tyrosine kinase RON, MSP-RON can activate two signaling pathways: RAS–ERK and PI3K–AKT, which were altered in 68% of recurrent glioma patients[21]. However, Bai, et al.[21] also reported there was a weak association of RTK-RAS-PI3K pathway activation with treatment (q = 0.05). Our case favored the perspective that RTK-RAS-PI3K pathway activation was a genomic event that underlines glioma progression rather than a selection result of treatment.

In the prespective of immune defending, immune microenvironment analysis revealed that the infiltration levels of CD4 + memory T cells and CD8 + T cells were lower in G4, and signal pathways including IL17 and cytotoxic T cell were down-regulated in G4, indicating the immune suppression of T cell response. this result was a little different from the report of Mohme, et al[22]. They found CD8 + T cell fraction was significantly higher in recurrent GBM than primary LGG, while CD4 + T cell fraction was significantly lower. The discordance of CD8 + T cell infiltration reveals the unique immune microenvironmental feature during evolution without artificial interference. We also detected the up-regulation of the NF-κB pathway in G4, activation of which could enhance cancer cell proliferation and induce immunosuppression[49].

Furthermore, Mohme, et al.[22] have found that the single most expanded clonotype occupied a significantly greater space in the recurrent GBM TIL, especially a few top-ranked clonotypes of which clone frequency can be higher than 15%. In our case, clone frequencies of the top two clonotypes were separately 38% and 19% in G2 and were separately 24% and 11% in G4, which were higher than those reported previously. The reason may be that the patient in our case was a long- term tumor carrier. Inderberg and colleagues[50] proposed long-term surviving cancer patients as a source of therapeutic TCR. The top two TCRs discovered in our case may have a great value in adoptive cell therapy of glioma.

In conclusion, we discovered biological processes including mutation of *CIC*, *BRCA2*, and *NAF1*, activation of MSP-RON and NF-κB pathways, and immune evasion contribute to the natural evolution of glioma. We identified two highly expanded TCR clonotypes that may recognize and eliminate glioma cells and may serve as potential adoptive cell therapy sources.

Declarations

Acknowledgments

The authors thank Dr. Min Shi for advice in the analysis framework.

Funding

This work supported by the National Natural Science Foundation of China (No.81672783).

Conflicts of interest/Competing interests

The authors declare that there is no conflict of interest.

Ethics approval

This study was approved by the ethics committee of Southwest Hospital, Army Medical University Chongqing,China.

Availability of data and material

Data were available upon appropriate request.

Authors' contributions

Long Wang and Feilong Zhao performed data analysis, interpretation, and visualization. And they wrote the manuscript. Xuegang Li and Tunan Chen conducted high-throughout sequencing. Hua Feng participated in the study design. Tonghui Ma participated in the study design and data interpretation. Fei Li designed and supervised the study, and revised the manuscript.

References

1. Masui K, Mischel PS, Reifenberger G. Molecular classification of gliomas. Handb Clin Neurol 2016;134:97-120
2. Louis DN, Perry A, Reifenberger G, von Deimling A, Figarella-Branger D, Cavenee WK*, et al.* The 2016 World Health Organization Classification of Tumors of the Central Nervous System: a summary. Acta Neuropathol 2016;131:803-20
3. Eckel-Passow JE, Lachance DH, Molinaro AM, Walsh KM, Decker PA, Sicotte H*, et al.* Glioma Groups Based on 1p/19q, IDH, and TERT Promoter Mutations in Tumors. N Engl J Med 2015;372:2499-508
4. Cancer Genome Atlas Research N, Brat DJ, Verhaak RG, Aldape KD, Yung WK, Salama SR*, et al.* Comprehensive, Integrative Genomic Analysis of Diffuse Lower-Grade Gliomas. N Engl J Med 2015;372:2481-98
5. Verhaak RG, Hoadley KA, Purdom E, Wang V, Qi Y, Wilkerson MD*, et al.* Integrated genomic analysis identifies clinically relevant subtypes of glioblastoma characterized by abnormalities in PDGFRA, IDH1, EGFR, and NF1. Cancer Cell 2010;17:98-110
6. Phillips HS, Kharbanda S, Chen R, Forrest WF, Soriano RH, Wu TD*, et al.* Molecular subclasses of high-grade glioma predict prognosis, delineate a pattern of disease progression, and resemble stages in neurogenesis. Cancer Cell 2006;9:157-73
7. Ozawa T, Riester M, Cheng YK, Huse JT, Squatrito M, Helmy K*, et al.* Most human non-GCIMP glioblastoma subtypes evolve from a common proneural-like precursor glioma. Cancer Cell 2014;26:288-300
8. Brennan C, Momota H, Hambardzumyan D, Ozawa T, Tandon A, Pedraza A*, et al.* Glioblastoma subclasses can be defined by activity among signal transduction pathways and associated genomic

alterations. PLoS One 2009;4:e7752

9. Sottoriva A, Spiteri I, Piccirillo SG, Touloumis A, Collins VP, Marioni JC*, et al.* Intratumor heterogeneity in human glioblastoma reflects cancer evolutionary dynamics. Proc Natl Acad Sci U S A 2013;110:4009-14
10. Malta TM, de Souza CF, Sabedot TS, Silva TC, Mosella MS, Kalkanis SN*, et al.* Glioma CpG island methylator phenotype (G-CIMP): biological and clinical implications. Neuro Oncol 2018;20:608-20
11. LeBlanc VG, Marra MA. DNA methylation in adult diffuse gliomas. Brief Funct Genomics 2016;15:491-500
12. Turcan S, Rohle D, Goenka A, Walsh LA, Fang F, Yilmaz E*, et al.* IDH1 mutation is sufficient to establish the glioma hypermethylator phenotype. Nature 2012;483:479-83
13. Noushmehr H, Weisenberger DJ, Diefes K, Phillips HS, Pujara K, Berman BP*, et al.* Identification of a CpG island methylator phenotype that defines a distinct subgroup of glioma. Cancer Cell 2010;17:510-22
14. Ceccarelli M, Barthel FP, Malta TM, Sabedot TS, Salama SR, Murray BA*, et al.* Molecular Profiling Reveals Biologically Discrete Subsets and Pathways of Progression in Diffuse Glioma. Cell 2016;164:550-63
15. Ohgaki H, Kleihues P. The definition of primary and secondary glioblastoma. Clin Cancer Res 2013;19:764-72
16. Louis DN, Ohgaki H, Wiestler OD, Cavenee WK, Burger PC, Jouvet A*, et al.* The 2007 WHO classification of tumours of the central nervous system. Acta Neuropathol 2007;114:97-109
17. Hu H, Mu Q, Bao Z, Chen Y, Liu Y, Chen J*, et al.* Mutational Landscape of Secondary Glioblastoma Guides MET-Targeted Trial in Brain Tumor. Cell 2018;175:1665-78 e18
18. Nobusawa S, Watanabe T, Kleihues P, Ohgaki H. IDH1 mutations as molecular signature and predictive factor of secondary glioblastomas. Clin Cancer Res 2009;15:6002-7
19. Wang J, Cazzato E, Ladewig E, Frattini V, Rosenbloom DI, Zairis S*, et al.* Clonal evolution of glioblastoma under therapy. Nat Genet 2016;48:768-76
20. Lee JK, Wang J, Sa JK, Ladewig E, Lee HO, Lee IH*, et al.* Spatiotemporal genomic architecture informs precision oncology in glioblastoma. Nat Genet 2017;49:594-9
21. Bai H, Harmanci AS, Erson-Omay EZ, Li J, Coskun S, Simon M*, et al.* Integrated genomic characterization of IDH1-mutant glioma malignant progression. Nat Genet 2016;48:59-66
22. Mohme M, Schliffke S, Maire CL, Runger A, Glau L, Mende KC*, et al.* Immunophenotyping of Newly Diagnosed and Recurrent Glioblastoma Defines Distinct Immune Exhaustion Profiles in Peripheral and Tumor-infiltrating Lymphocytes. Clin Cancer Res 2018;24:4187-200
23. Jacobs JF, Idema AJ, Bol KF, Nierkens S, Grauer OM, Wesseling P*, et al.* Regulatory T cells and the PD-L1/PD-1 pathway mediate immune suppression in malignant human brain tumors. Neuro Oncol 2009;11:394-402

24. Fecci PE, Mitchell DA, Whitesides JF, Xie W, Friedman AH, Archer GE*, et al.* Increased regulatory T-cell fraction amidst a diminished CD4 compartment explains cellular immune defects in patients with malignant glioma. Cancer Res 2006;66:3294-302
25. Fecci PE, Heimberger AB, Sampson JH. Immunotherapy for primary brain tumors: no longer a matter of privilege. Clin Cancer Res 2014;20:5620-9
26. Dyck L, Mills KHG. Immune checkpoints and their inhibition in cancer and infectious diseases. Eur J Immunol **2017**;47:765-79
27. Zisakis A, Piperi C, Themistocleous MS, Korkolopoulou P, Boviatsis EI, Sakas DE*, et al.* Comparative analysis of peripheral and localised cytokine secretion in glioblastoma patients. Cytokine 2007;39:99-105
28. Li Z, Liu X, Guo R, Wang P. CD4(+)Foxp3(-) type 1 regulatory T cells in glioblastoma multiforme suppress T cell responses through multiple pathways and are regulated by tumor-associated macrophages. Int J Biochem Cell Biol 2016;81:1-9
29. Raychaudhuri B, Rayman P, Ireland J, Ko J, Rini B, Borden EC*, et al.* Myeloid-derived suppressor cell accumulation and function in patients with newly diagnosed glioblastoma. Neuro Oncol 2011;13:591-9
30. McKenna A, Hanna M, Banks E, Sivachenko A, Cibulskis K, Kernytsky A*, et al.* The Genome Analysis Toolkit: a MapReduce framework for analyzing next-generation DNA sequencing data. Genome Res 2010;20:1297-303
31. Cibulskis K, Lawrence MS, Carter SL, Sivachenko A, Jaffe D, Sougnez C*, et al.* Sensitive detection of somatic point mutations in impure and heterogeneous cancer samples. Nat Biotechnol 2013;31:213-9
32. Saunders CT, Wong WS, Swamy S, Becq J, Murray LJ, Cheetham RK. Strelka: accurate somatic small-variant calling from sequenced tumor-normal sample pairs. Bioinformatics 2012;28:1811-7
33. Andor N, Harness JV, Muller S, Mewes HW, Petritsch C. EXPANDS: expanding ploidy and allele frequency on nested subpopulations. Bioinformatics 2014;30:50-60
34. Malikic S, McPherson AW, Donmez N, Sahinalp CS. Clonality inference in multiple tumor samples using phylogeny. Bioinformatics 2015;31:1349-56
35. Fra Paleo U. Timescape of disaster risk governance in contemporary Japan: Neither state of normalcy nor constancy in regulation. PLoS One 2019;14:e0215164
36. Yoshihara K, Shahmoradgoli M, Martinez E, Vegesna R, Kim H, Torres-Garcia W*, et al.* Inferring tumour purity and stromal and immune cell admixture from expression data. Nat Commun 2013;4:2612
37. Hanzelmann S, Castelo R, Guinney J. GSVA: gene set variation analysis for microarray and RNA-seq data. BMC Bioinformatics 2013;14:7
38. Subramanian A, Tamayo P, Mootha VK, Mukherjee S, Ebert BL, Gillette MA*, et al.* Gene set enrichment analysis: a knowledge-based approach for interpreting genome-wide expression profiles. Proc Natl Acad Sci U S A 2005;102:15545-50

39. Cahoy JD, Emery B, Kaushal A, Foo LC, Zamanian JL, Christopherson KS*, et al.* A transcriptome database for astrocytes, neurons, and oligodendrocytes: a new resource for understanding brain development and function. J Neurosci 2008;28:264-78
40. Aryee MJ, Jaffe AE, Corrada-Bravo H, Ladd-Acosta C, Feinberg AP, Hansen KD*, et al.* Minfi: a flexible and comprehensive Bioconductor package for the analysis of Infinium DNA methylation microarrays. Bioinformatics 2014;30:1363-9
41. Teschendorff AE, Marabita F, Lechner M, Bartlett T, Tegner J, Gomez-Cabrero D*, et al.* A beta-mixture quantile normalization method for correcting probe design bias in Illumina Infinium 450 k DNA methylation data. Bioinformatics 2013;29:189-96
42. Du P, Zhang X, Huang CC, Jafari N, Kibbe WA, Hou L*, et al.* Comparison of Beta-value and M-value methods for quantifying methylation levels by microarray analysis. BMC Bioinformatics 2010;11:587
43. Bady P, Sciuscio D, Diserens AC, Bloch J, van den Bent MJ, Marosi C*, et al.* MGMT methylation analysis of glioblastoma on the Infinium methylation BeadChip identifies two distinct CpG regions associated with gene silencing and outcome, yielding a prediction model for comparisons across datasets, tumor grades, and CIMP-status. Acta Neuropathol 2012;124:547-60
44. Bady P, Delorenzi M, Hegi ME. Sensitivity Analysis of the MGMT-STP27 Model and Impact of Genetic and Epigenetic Context to Predict the MGMT Methylation Status in Gliomas and Other Tumors. J Mol Diagn 2016;18:350-61
45. Wang X, Hu Y, Liu X, Yu J, Xu P, Wei G*, et al.* Quantitative characterization of T-cell repertoire alteration in Chinese patients with B-cell acute lymphocyte leukemia after CAR-T therapy. Bone Marrow Transplant 2019;54:2072-80
46. Yao HP, Zhou YQ, Zhang R, Wang MH. MSP-RON signalling in cancer: pathogenesis and therapeutic potential. Nat Rev Cancer 2013;13:466-81
47. Chen B, Khodadoust MS, Liu CL, Newman AM, Alizadeh AA. Profiling Tumor Infiltrating Immune Cells with CIBERSORT. Methods Mol Biol 2018;1711:243-59
48. Wei J, Yang Q, Shi J, Shi B, Ji M, Hou P. Increased expression of NAF1 contributes to malignant phenotypes of glioma cells through promoting protein synthesis and associates with poor patient survival. Oncogenesis 2019;8:25
49. Taniguchi K, Karin M. NF-kappaB, inflammation, immunity and cancer: coming of age. Nat Rev Immunol 2018;18:309-24
50. Inderberg EM, Walchli S. Long-term surviving cancer patients as a source of therapeutic TCR. Cancer Immunol Immunother 2020;69:859-65

Tables

Table 1. Clone fraction and representative mutations assigned

Clone_id	Clonal_prevalence_G2	clonal_prevalence_G4	Representive_mutations
1	0.27	0.08	IDH1, TP53, NAF1
2	0.00	0.29	NOTCH1(p.A1967V)
3	0.04	0.01	APOB
4	0.01	0.31	CIC, BRCA2, HMCN1
5	0.00	0.14	FFAR1
6	0.29	0.01	RBPJ
7	0.12	0.00	NOTCH1(p.Q310R)

Figures

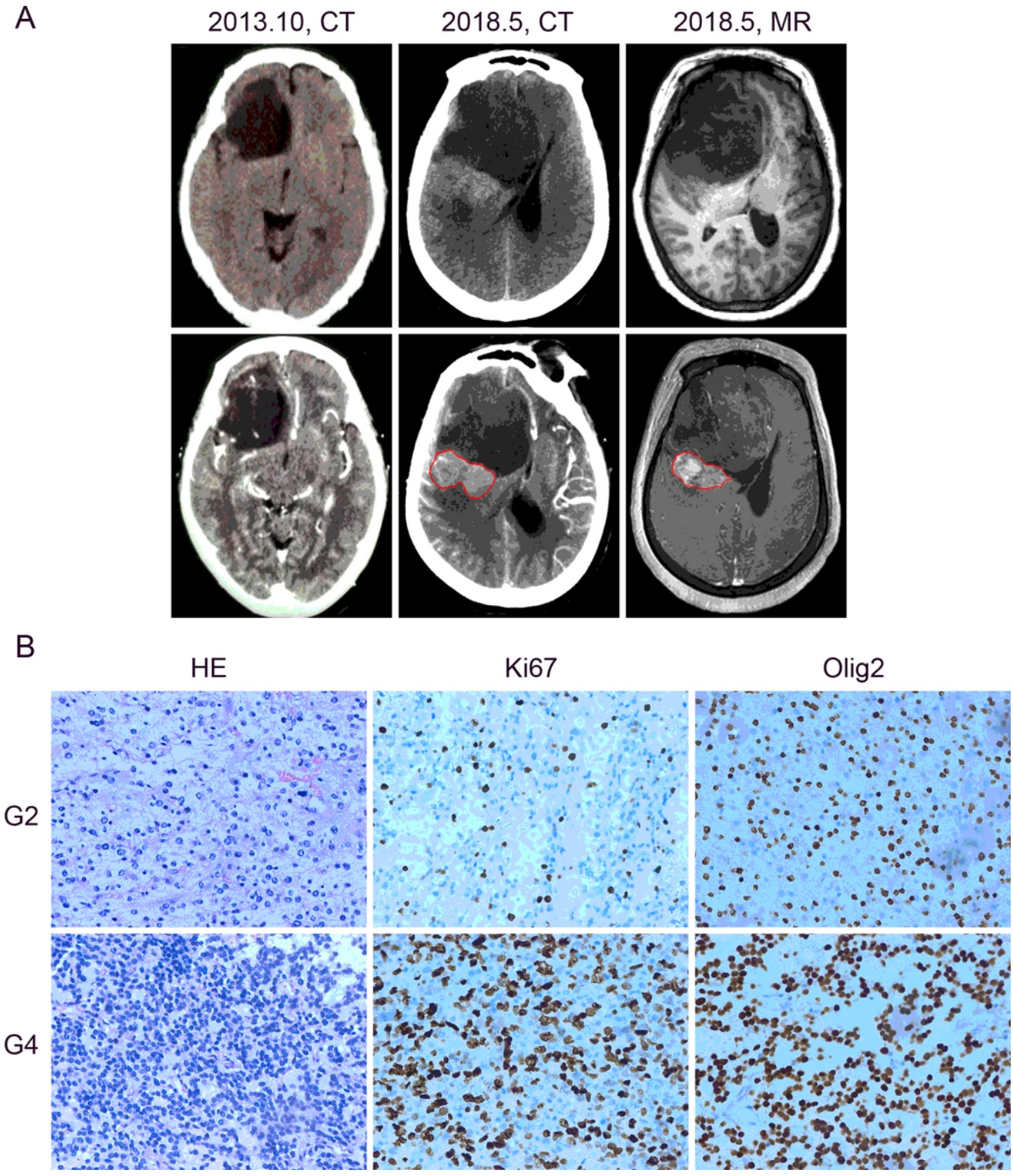

Figure 1

Imagological and histological diagnosis of the patient. A. In October 2013, a low-density area with a suborbicular shadow was detected at the right frontal lobe, but no significant enhancement was discovered in CT (the left panel). In May 2018, CT (middle panel) and MR (right panel) examination showed that the primary was enlarged, lateral ventricle shifted towards left under pressure, and a new enhanced shadow (outlined by the red circle) was discovered at the posterior of the tumor. B. HE, Anti-

Ki67, and Anti-Olig2 staining of the primary (G2) and secondary (G4) glioma samples. Brown circles represent positive staining.

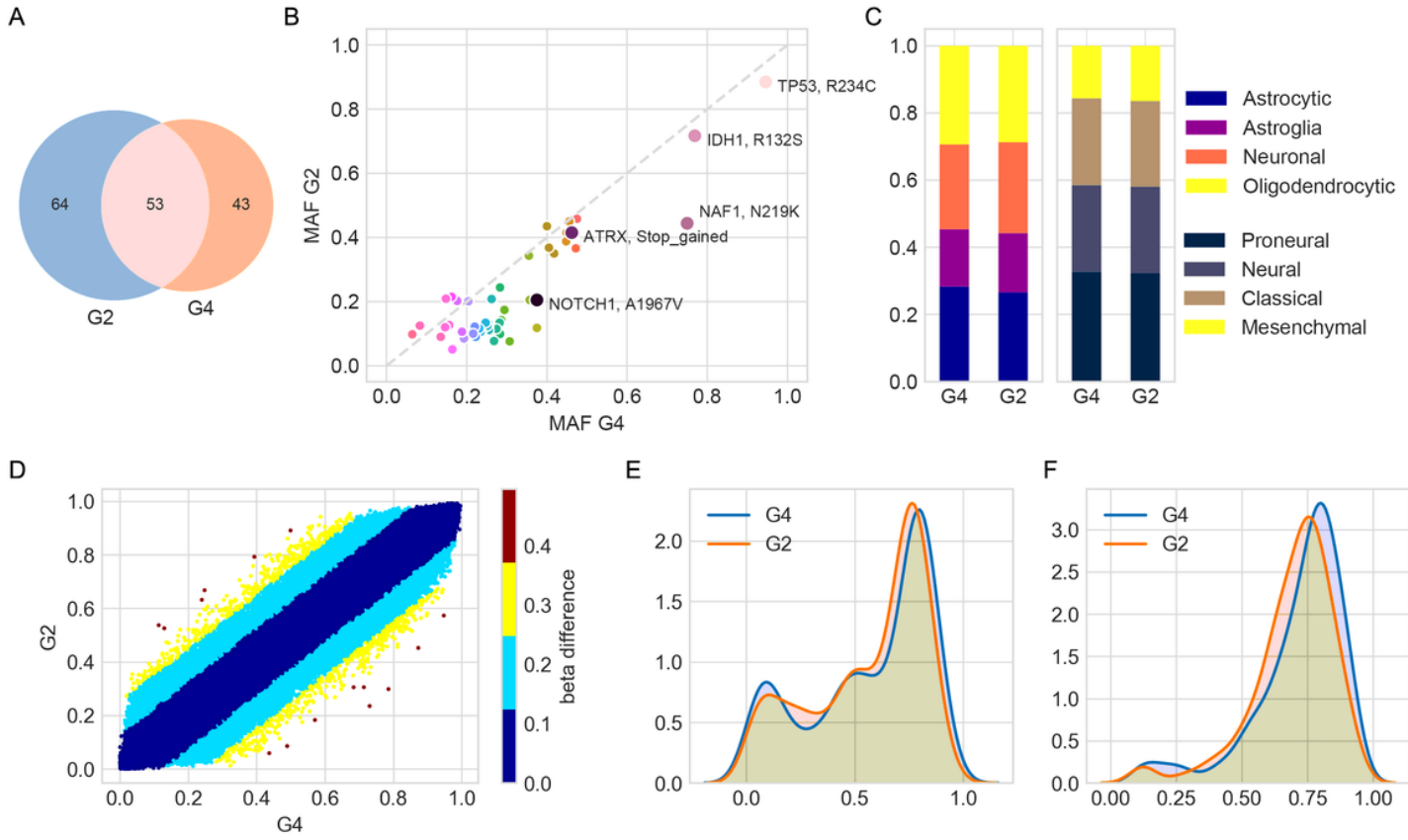

Figure 2

Molecular characteristics of G2 and G4. A. Venn plot of the private and common mutations of G2 and G4. B. MAFs of shared mutations between G2 and G4. C. Cell origins and transcription subtypes of G2 and G4 analyzed by ssGSEA using signatures previously reported. D. Beta-values of shared probes between G2 and G4 at probes level. Each point represents a probe, the colorbar illustrated the difference of beta-values between the two samples. E. Density plot of the 1503 probes used to define CIMP. F. Density plot of the 131 probes used to define CIMP-High.

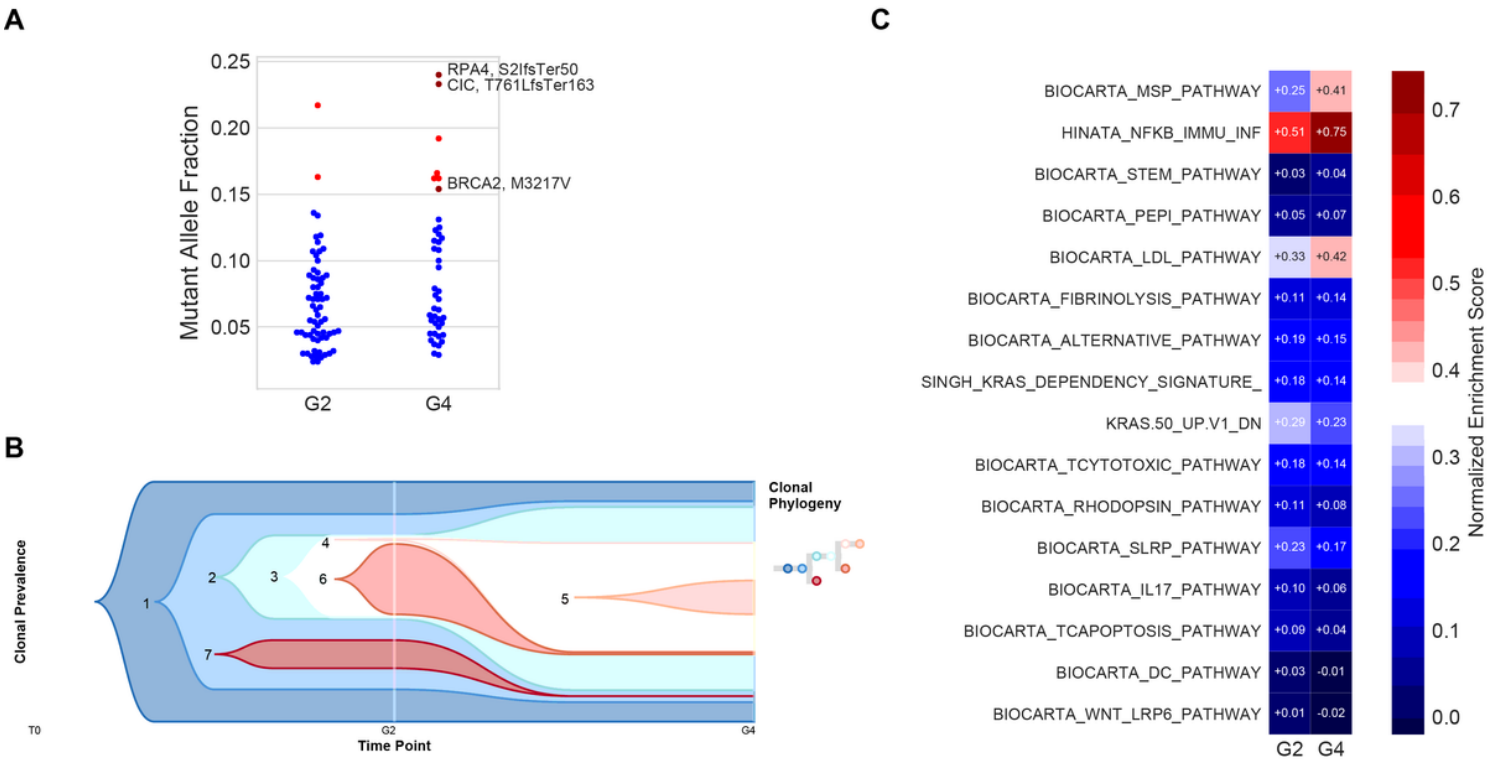

Figure 3

Evolution trajectory from G2 to G4. A. Private mutation and their MAFs in G2 and G4, with CIC, BRCA2, and RPA4 mutations annotated. B. Clonal evolution from G2 to G4, the seven clones were labeled as 1 to 7. C. Normalized enrichment score of pathways analyzed using expression matrix of G2 and G4. The score was illustrated in the colorbar.

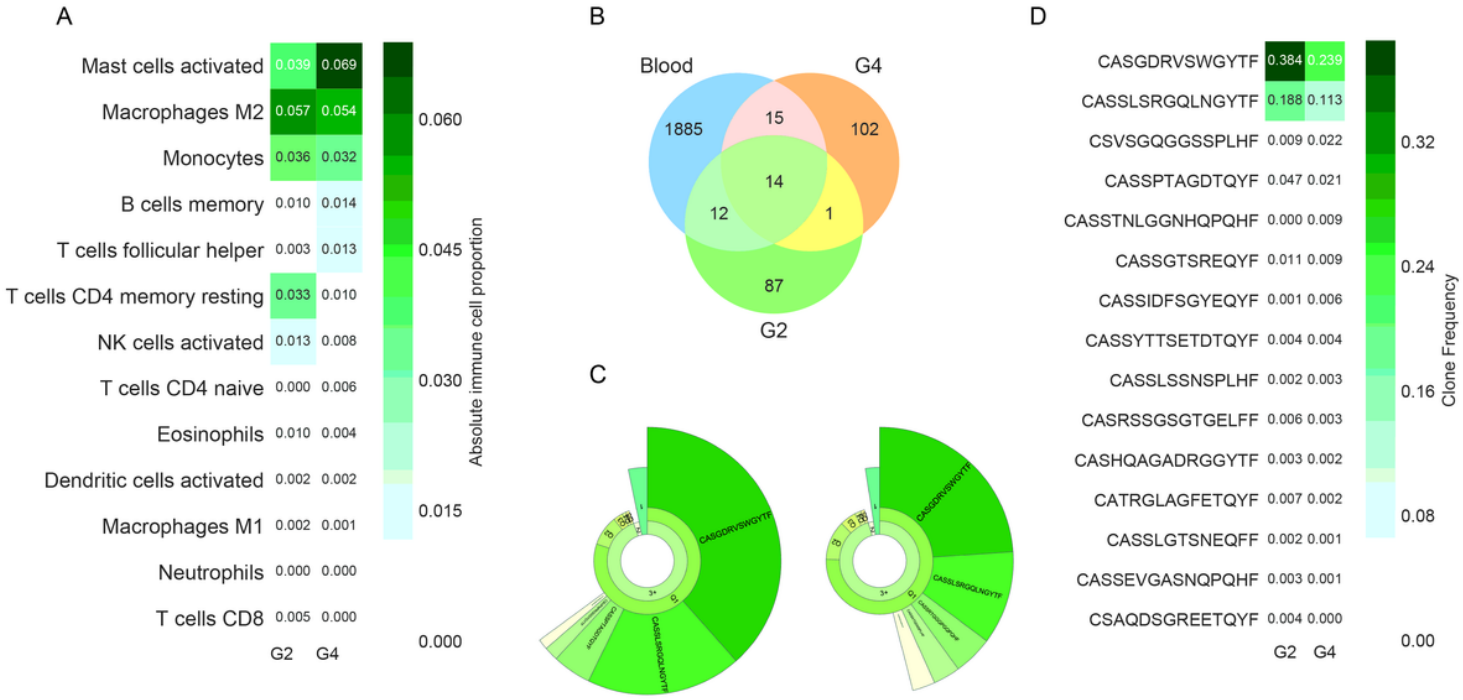

Figure 4

Immune microenvironment alteration concomitant with tumor evolution. A. The absolute fraction of the thirteen types of immune cells in bulk tissues of G2 and G4. B. Private and shared TCR clonotypes of G2, G4, and peripheral blood. C. A representative donut chart of G2 and G4 displays the clonal expansion. The fan-shaped area displays the corresponding clonal frequency. The radian of 1, 2, and 3+ represented the total frequency of TCR sequences having 1, 2, and 3 more reads, respectively. The top 5 clones' amino acid sequences of complementary determination region 3 (CDR3) of TCR were shown in the donut chart and the radian of the region which was marked with the amino acid sequence demonstrated the frequency of the corresponding T cell clones. The larger radian means higher frequency. D. Clone frequency of the fifteen shared clonotypes between G2 and G4. The greener the color is, the higher the clone fraction.